

Electronic Supplementary Information

Bundled-Stack Discotic Columnar Liquid Crystalline Phase with Inter-Stack Electronic Coupling

Bin Wang,[†] Runkun Sun,[†] D. Deniz Günbaş,[§] Hao Zhang,[†] Ferdinand C. Grozema,[§] Kai Xiao[‡] and Shi Jin^{*†}

[†]*Center for Engineered Polymeric Materials, Department of Chemistry, College of Staten Island and Graduate Center of the City University of New York, Staten Island, NY 10314 (USA).*

[§]*DelftChemTech, Delft University of Technology, Julianalaan 136, 2628 BL Delft (Netherland).*

[‡]*Center for Nanophase Materials Sciences and Materials Science and Technology Division, Oak Ridge National Laboratory, One Bethel Valley Road, Oak Ridge, TN 37831 (USA).*

*Email: shi.jin@csi.cuny.edu

Table of contents

1. Materials.....	Page S3
2. Sample characterization.....	Page S3
3. Synthesis and NMR spectra.....	Page S5
4. Summary of WAXD diffraction positions of PEA 1 and PEI 2	Page S12
5. Polarized light microscopic pictures of PEA 1	Page S13
6. UV-Visible spectra of PEA 1 and PEI 2	Page S14
7. Fluorescence spectra of PEA 1	Page S17
8. FT-IR spectra of LC film and hexane solutions of PEA 1	Page S17
9. DSC traces and 1D and 2D X-ray diffraction patterns of PEI 2	Page S18
10. Frontier molecular orbitals and inter-stack orbital overlap.....	Page S20
11. Detailed simulation procedure.....	Page S21
12. Discussion on the role of flexible long alkyl peripheral chains.....	Page S26
13. Conductivity transient of PEA 1 in RT BSDCLC phase by measured by PR-TRMC.....	Page S28
14. References.....	Page S29

1. Materials

All reagents and chemicals were purchased from Fisher Scientific, Aldrich or VWR international and used as received. ALIQUAT® 336 was kindly provided by Cognis Corporation.

2. Sample characterization

¹H NMR and ¹³C spectra were recorded on a Varian 600 MHz NMR spectrometer, with deuterated chloroform (CDCl₃) as solvent at 25 °C. The chemical shifts were reported using chloroform as the internal standard. The ¹H NMR and ¹³C NMR graphs and data were scanned and calculated from original graphs.

Samples that were studied in their DCLC phase were heated to isotropic state before cooling to the mesophase to eliminate the thermal history. In some cases (e.g. POM pictures), samples were annealed at high temperature followed by slow cooling with controlled rate.

High resolution mass spectrum (HRMS) of **1** was obtained in Chemistry Department at Rutgers University Newark on an Apex-ultra 70 hybrid Fourier Transform mass spectrometer (Bruker Daltonics).

FT-IR spectra were collected on a Bruker Vertex 70V spectrometer with transmission set up at a resolution of 1 cm⁻¹. Liquid N₂ cooled MCT detector was employed to achieve optimal signal to noise ratio. Sample compartment was vacuumed for the measurement of solid samples and was purged with N₂ gas for solutions.

UV-visible spectra were obtained on a PerkinElmer Lambda 650 UV/Vis spectrophotometer with the resolution of 1 nm. 1 cm glass cell was used for hexane or chloroform solutions of **1** and **2** with concentrations lower than 1×10⁻⁴ M. For higher concentration, a 0.5 mm quartz cell was used for spectrum collection. All solid (LC) samples were coated on a quartz plate for measurements.

Fluorescence spectra were collected on a JOBIN YVON Co. FluoroMax-3 spectrofluorometer. The excitation wavelengths were determined by absorption spectra before measurements.

Table S1. Concentrations of hexane solutions of PEA **1**

Number of solution	1	2	3	4	5	6	7	8
Concentration (M)	9.69×10 ⁻⁵	6.87×10 ⁻⁵	4.73×10 ⁻⁵	3.52×10 ⁻⁵	2.35×10 ⁻⁵	1.73×10 ⁻⁵	1.13×10 ⁻⁵	8.69×10 ⁻⁶

All X-ray diffraction measurements were performed on a Bruker Nanostar instrument with a Cu K_a source. A VÅNTEC 2000 2D detector and an image plate were used as small and wide angle detectors, respectively. The wide angle powder diffraction pattern shown in Figure 1 was collected from 1 mm thick **1** sample with Si powder as internal d-spacing reference. The 2D small angle diffraction pattern shown in Figure 1f was obtained by aligning the X-ray incident beam along the axis of supramolecular columns in a millimeter-sized homeotropically aligned single domain liquid crystalline sample of **1**. To prepare such a sample suitable for X-ray measurement, the raw material was sandwiched between two freshly cleaved sodium chloride plates which provide smooth surfaces. In addition, sodium chloride could be removed by dissolving in water to obtain the substrate-free thin film of **1** for the X-ray experiment. The sample was heated up to isotropic state and cooled down stepwise initially (step size 0.1 °C). The cooling was paused at each step to find the exact temperature point at which the texture starts to develop. The sample was then annealed at this temperature for about 10 minutes followed by slow cooling (0.1 °C /min), leading to the formation of ~ 1 mm × 2 mm single domain. Consequently, the sample was cooled to room temperature at 5 °C/min followed by dissolving sodium chloride in water. Unlike electron diffraction with TEM, X-ray beam covers an area about 1 mm² in size which enables us to probe the global alignment of a sample film. The cooling profile described here is applicable on surfaces such as NaCl plates, ordinary glass and ITO coated glass, etc. to yield homeotropically aligned thin films of **1**. The diffraction pattern shown in Figure 2 was obtained by aligning the incident X-ray beam perpendicular to the plane of a mechanically sheared film of **1** with the shearing direction pointing upwards.

Polarized light microscopy pictures shown in Figure 1d, 4b were taken from a Leica DM LB2 microscope equipped with a Leica DGC 320 camera and a Mettler Toledo FP82HT hotstage (controlled by a Mettler Toledo FP90 central processor). Samples were heated up to the isotropic liquid state then cooled down to desired temperature with a cooling rate of 0.1 °C/min.

DSC experiments were performed on a Perkin-Elmer PYRIS Diamond differential scanning calorimeter or a TA Q20 differential scanning calorimeter. Transition temperatures were determined using the onset temperatures and were calibrated using standard material (indium).

The mobility of charges in PEA **1** was determined by PR-TRMC measurements. PR-TRMC technique has been extensively described elsewhere.¹ Briefly, the sample is irradiated with a short pulse of high-energy (3 MeV)

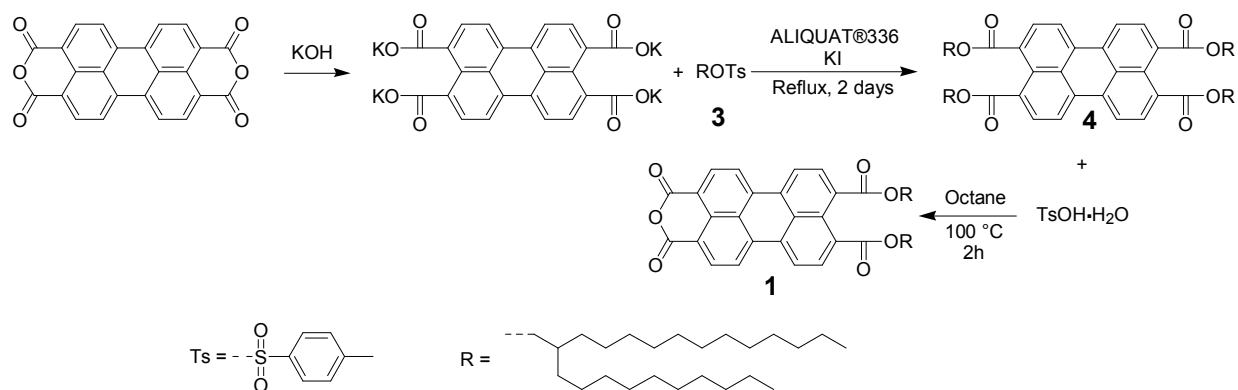
electrons from a Van de Graaf accelerator, which leads initially to a low (micromolar) concentration of positive and negative charge carriers uniformly distributed in the irradiated medium. After the incident pulse (1 – 50 ns duration), the conductivity of the sample is probed as a function of time by monitoring the attenuation of a reflected microwave power (frequency range between 28 and 38 GHz, maximum electric field strength in the sample 10 V/m). The fractional change in microwave power reflected by the cell is directly proportional to the change in conductivity, $\Delta\sigma$. The concentration of charges that is generated initially can be estimated using dosimetry measurements² combined with a charge-scavenging model. The sum of the one-dimensional intracolumnar charge carrier mobilities from the dose-normalized radiation-induced conductivity at the end-of-the-pulse, $\Delta\sigma/D$, is determined according to the following equation:

$$\Sigma\mu = 3 \frac{\Delta\sigma E_p}{D W_p}$$

where E_p average energy absorbed per electron-hole pair formed and W_p is the probability that initially formed ion-pairs survive until the end of the pulse. The value of E_p is generally assumed to be ca. 25 eV and the value of W_p , acquired as described in ref.3, was 0.459. Because both positive and negative charge carriers can contribute to the conductivity signal, $\Sigma\mu$ represents the sum of hole and electron mobility.

3. Synthesis

Synthesis procedure for PEA **1** is outlined below:



2-decyltetradecyl 4-methylbenzenesulfonate (3)

3 was synthesized according to a literature procedure.⁴ A 100 ml round-bottomed flask was charged with 14.16 g (40 mmol) 2-decyl-1-tetradecanol, 12.12 g (120 mmol) triethylamine, 0.76 g (8 mmol) trimethylamine

hydrochloride and 40 ml dichloromethane. Then the mixture was cooled and stirred in an ice-water bath for 20 minutes. Afterwards, 7.18 g (38 mmol) 4-methylbenzenesulfonyl chloride was dissolved in 10 ml dichloromethane and the solution was added in a dropwise fashion into the reaction flask using a constant pressure funnel. Care was taken to maintain the temperature of the ice-water bath at 0 °C during the reaction. The reaction progress was monitored by thin layer chromatography. The reaction was ended when 4-methylbenzenesulfonyl chloride was fully consumed and it took approximately 3 hours. Upon the completion of reaction, 14.5 g (150 mmol) phosphoric acid and 20 ml water were added into the reaction mixture. The mixture was stirred for 15 minutes. Then the dichloromethane phase was washed with 20 ml 0.1 M HCl and 30 ml water in a separatory funnel. Dichloromethane was then removed on a rotary evaporator. The liquid residue was purified by silica column chromatography with chloroform as the eluent. Yield **3** 18.05 g (95%), as a colorless liquid.

3,4,9,10-tetra-(2-decyltetradecyloxycarbonyl) perylene (4)

Into a 200 ml round-bottomed flask were added 1.568 g (4 mmol) 3,4,9,10-perylenetetracarboxyldianhydride, 1.122 g (20 mmol) potassium hydroxide and 60 ml deionized water. The mixture was purged with nitrogen when it was heated at 70 °C for 2 hours. Subsequently, the solution was filtered to another 200 ml round-bottomed flask. The pH value was then adjusted to 8-9 with 1M hydrochloric acid solution. Into the solution were added 1.616 g (~4 mmol) ALIQUAT® 336 and 0.06 g (0.4 mmol) potassium iodide. The mixture was stirred vigorously for 10 minutes followed by adding in 16 g (32 mmol) **3**. Then the solution was refluxed with vigorous stirring for 2 days. Afterwards, the green reaction mixture was extracted by portions of 20 ml chloroform until the chloroform phase is nearly colorless. The combined chloroform phase was then washed with brine for three times. After removing chloroform on a rotary evaporator, the liquid residue was precipitated into 200 ml methanol. The crude product was then collected with gravity filtration, washed twice with methanol and dried under vacuum at 50 °C overnight, yielding 3.24 g crude product **4** as a green, highly viscous liquid.

Perylene-3,4-anhydride-9,10-di-(2-decyltetradecyloxycarbonyl) (1)

Into a 50 ml round-bottomed flask were charged with 1.774 g crude **4**, 0.19 g (1 mmol) *p*-toluenesulfonic acid monohydrate and 10 ml *n*-octane. The mixture was then heated to 100 °C for 2 hours. The *n*-octane was later removed on a rotary evaporator. The red residue was collected by dissolving in 5 ml chloroform and then precipitated in methanol. After filtration, the crude product was purified by column chromatography with 50/1(v/v)

chloroform/acetone as the eluent, yielding **1** 0.324 g as a red solid. The overall yield calculated from 3,4,9,10-perylenetetracarboxyldianhydride is 14%.

¹H NMR (CDCl₃, 600 MHz): δ (ppm) = 8.62 (d, J = 7.98 Hz, 2H, Ar), 8.48 (m, 4H, Ar), 8.10 (d, J = 7.98 Hz, 2H, Ar), 4.26 (d, J = 6 Hz, 4H, -OCH₂CH), 1.83 (m, 2H, CH), 1.46 – 1.19 (m, 80 H, CH₂), 0.85 (m, 12 H, CH₃)

¹³C NMR (CDCl₃, 150 MHz): δ (ppm) = 168.07 (ester C=O), 160.30 (anhydride C=O), 137.59 (Ar), 133.56 (Ar), 132.93 (Ar), 131.86 (Ar), 131.39 (Ar), 130.16 (Ar), 129.30 (Ar), 126.38 (Ar), 123.49 (Ar), 122.04 (Ar), 117.94 (Ar), 68.69 (CO₂CH₂CH₂), 37.37 (CO₂CH₂CH), 31.95 (CH₂), 31.33 (CH₂), 30.02 (CH₂), 29.69 (CH₂), 29.39 (CH₂), 26.75 (CH₂), 22.69 (CH₂), 14.12 (CH₃)

FT-IR (cm⁻¹): 2925 (antisymmetric CH₂), 2854 (symmetric CH₂), 1770 (symmetric anhydride C=O), 1738 (antisymmetric anhydride C=O), 1711 (ester C=O), 1590 (aromatic ring stretch).

HRMS (M⁺e⁻): calcd for C₇₂H₁₀₆NO₇ 1083.7967; found 1083.7886. MALDI with benzopyrene as the matrix.

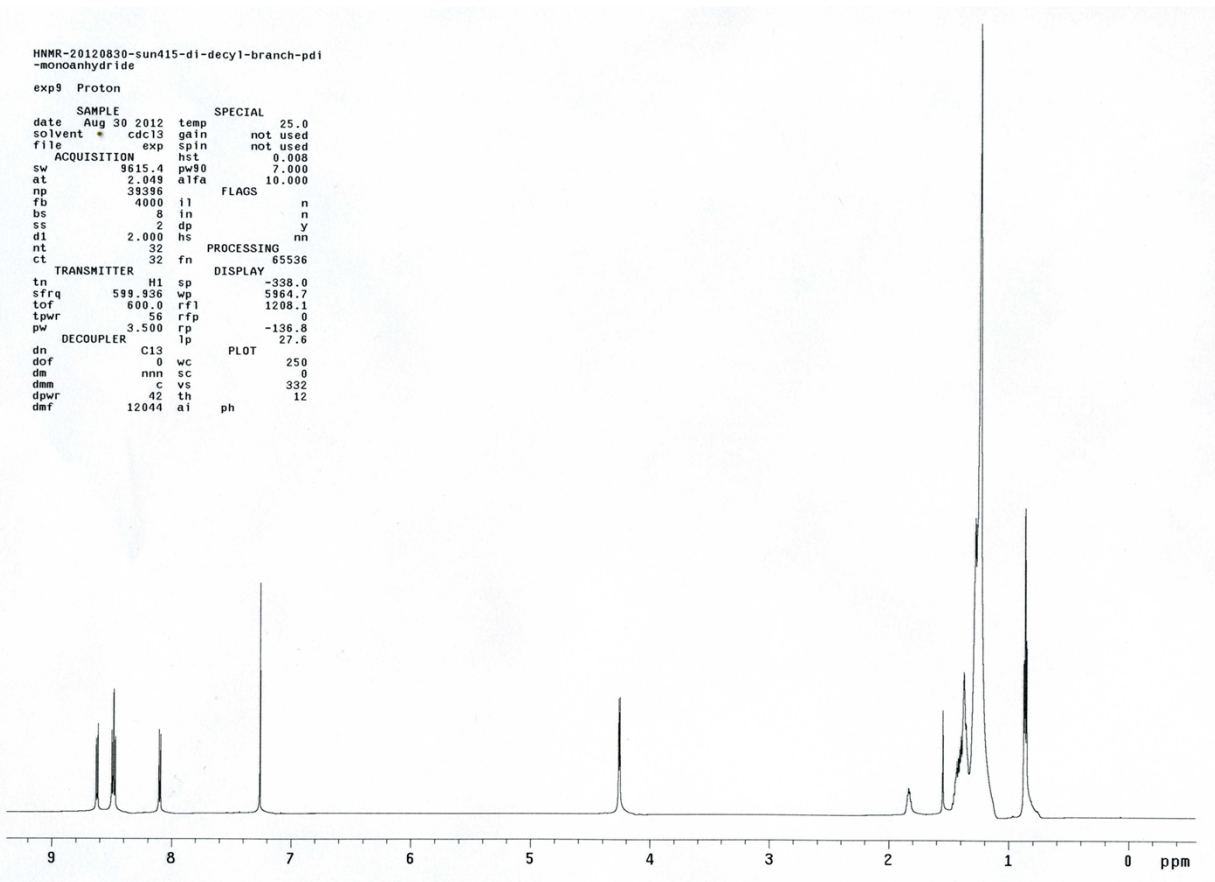


Figure S1. ¹H NMR spectrum of **1**

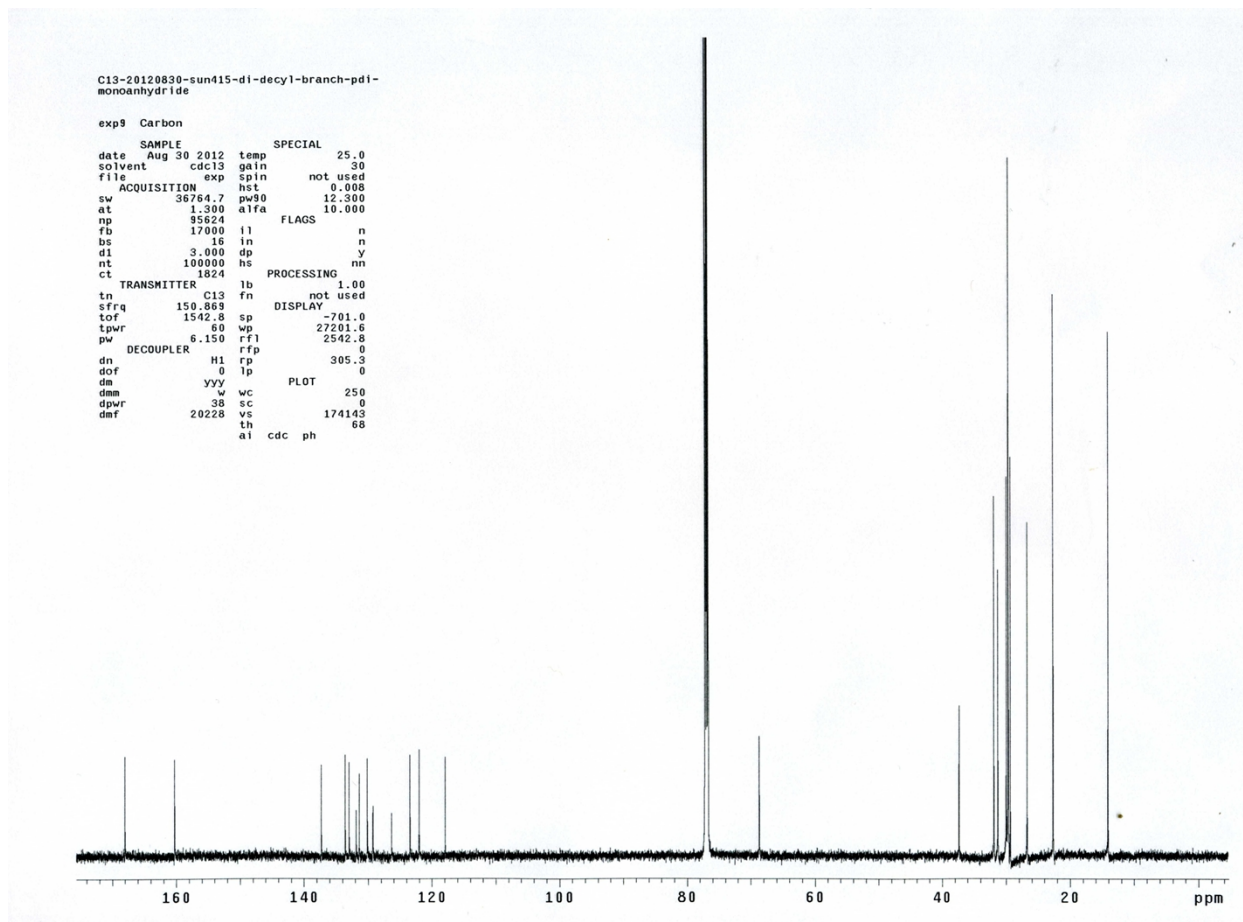
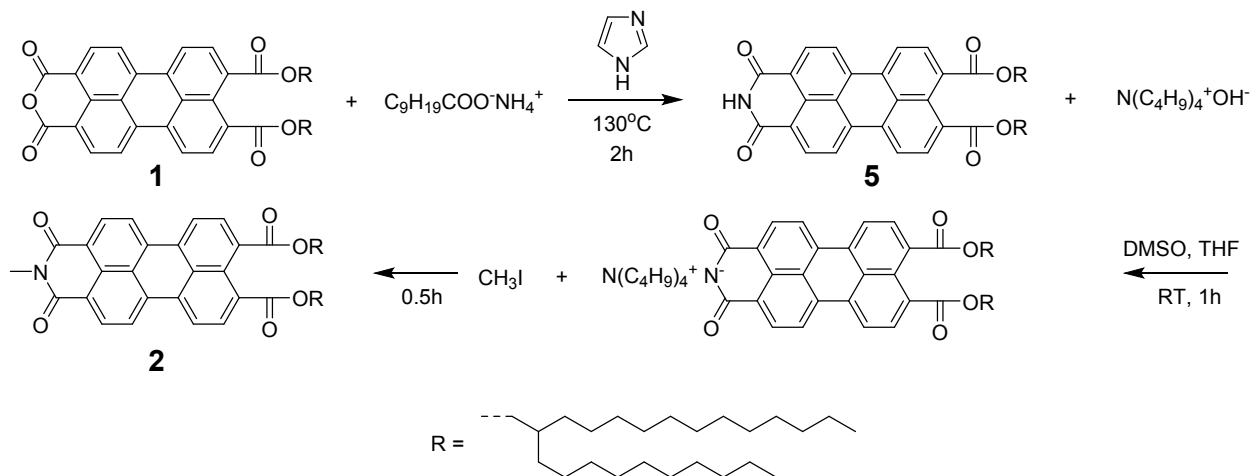


Figure S2. ^{13}C NMR spectrum of **1**

Synthesis procedure for PEI **2** is outlined below:



Perylene-3,4-dicarboximide-9,10-di-(2-decyltetradecyloxy carbonyl) (5)

Into a 10 ml round-bottomed flask were charged with 0.112 g (0.103 mmol) **1**, 0.069 g (0.365 mmol) ammonium decanoate and 1.2 g imidazole. The mixture was then heated to 130 °C with cap sealed for 2 hours. The reaction was terminated by cooling the mixture to 80 °C, followed by adding water to dissolve imidazole. Water phase was discarded by decant. The red residue was collected by dissolving in 5 ml chloroform and was purified by column chromatography with 50/1(v/v) chloroform/acetone as the eluent, yielding **5** 0.090 g (80%) as a red solid.

N-methyl-perylene-3,4-dicarboximide-9,10-di-(2-decyltetradecyloxy carbonyl) (2)

Into a 10 ml round-bottomed flask were charged with 0.040 g (0.0369 mmol) **5**, 0.016 g (0.0339 mmol) tetrabutyl ammonium hydroxide (55%, wt%), 1 ml THF and 2 ml DMSO. The mixture was stirred at RT for 1 hour under the protection of N₂ to ensure complete dissolution. Into the reaction container was added 0.011 g (0.0775 mmol) methyl iodide and stirred at RT with cap sealed for another 30 minutes. Solvents were removed by dissolving in water followed by decanting. The red residue was collected by dissolving in 5 ml chloroform and was purified by column chromatography with chloroform as the eluent, yielding **2** 0.021 g (51%) as a red solid.

¹H NMR (CDCl₃, 600 MHz): δ (ppm) = 8.66 (d, J = 7.82 Hz, 2H, Ar), 8.50 (m, 4H, Ar), 8.10 (d, J = 7.82 Hz, 2H, Ar), 4.25 (d, J = 6.60 Hz, 4H, -OCH₂CH), 3.598 (s, 3H, -NCH₃), 1.82 (m, 2H, CH), 1.47 – 1.19 (m, 80 H, CH₂), 0.86 (m, 12 H, CH₃).

¹³C NMR (CDCl₃, 150 MHz): δ (ppm) = 168.22 (ester C=O), 163.79 (imide C=O), 135.53 (Ar), 132.14 (Ar), 131.90 (Ar), 131.33 (Ar), 130.08 (Ar), 129.25 (Ar), 128.99 (Ar), 125.92 (Ar), 122.61 (Ar), 121.85 (Ar), 121.68 (Ar), 68.57 (CO₂CH₂CH₂), 37.37 (CO₂CH₂CH), 31.93 (CH₂), 31.34 (CH₂), 30.03 (CH₂), 29.70 (CH₂), 29.38 (CH₂), 27.05 (NCH₃), 26.77 (CH₂), 22.69 (CH₂), 14.11 (CH₃)

FT-IR (cm⁻¹): 2922 (antisymmetric CH₂), 2853 (symmetric CH₂), 1696 (symmetric imide C=O), 1657 (antisymmetric imide C=O), 1707 (ester C=O), 1594 (aromatic ring stretch).

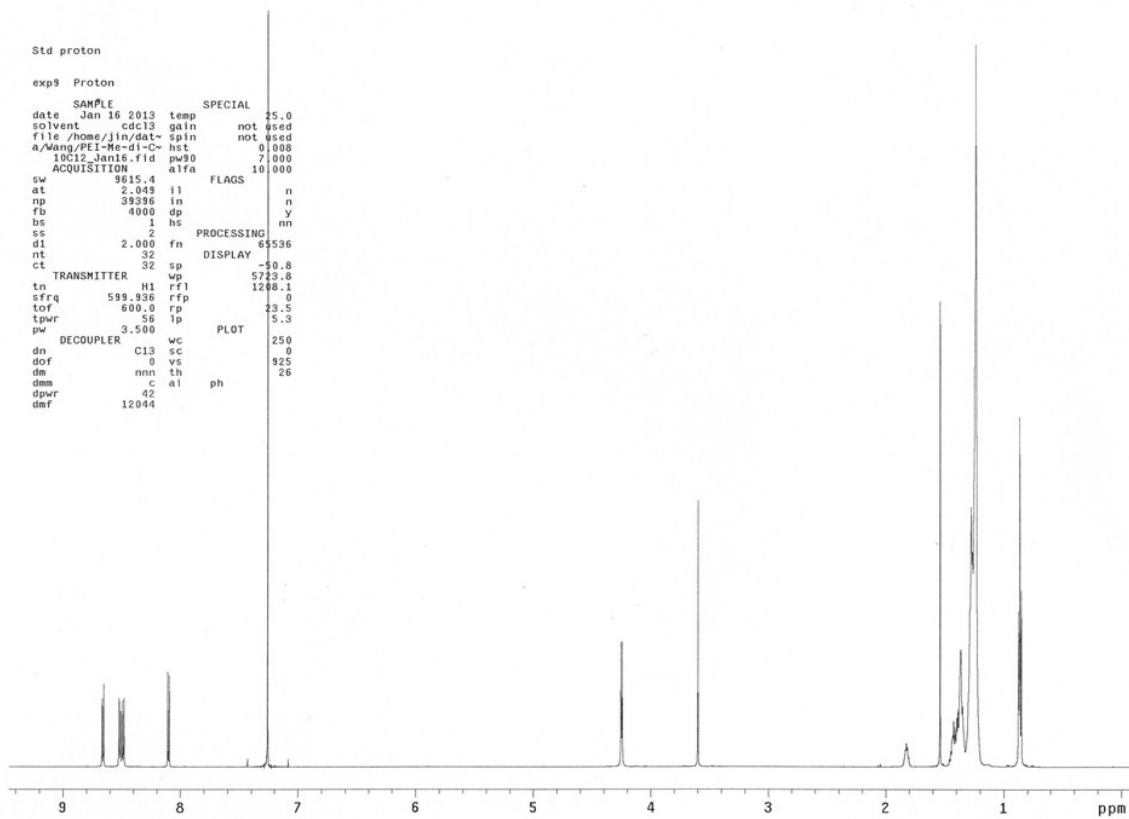


Figure S3. ^1H NMR spectrum of **2**

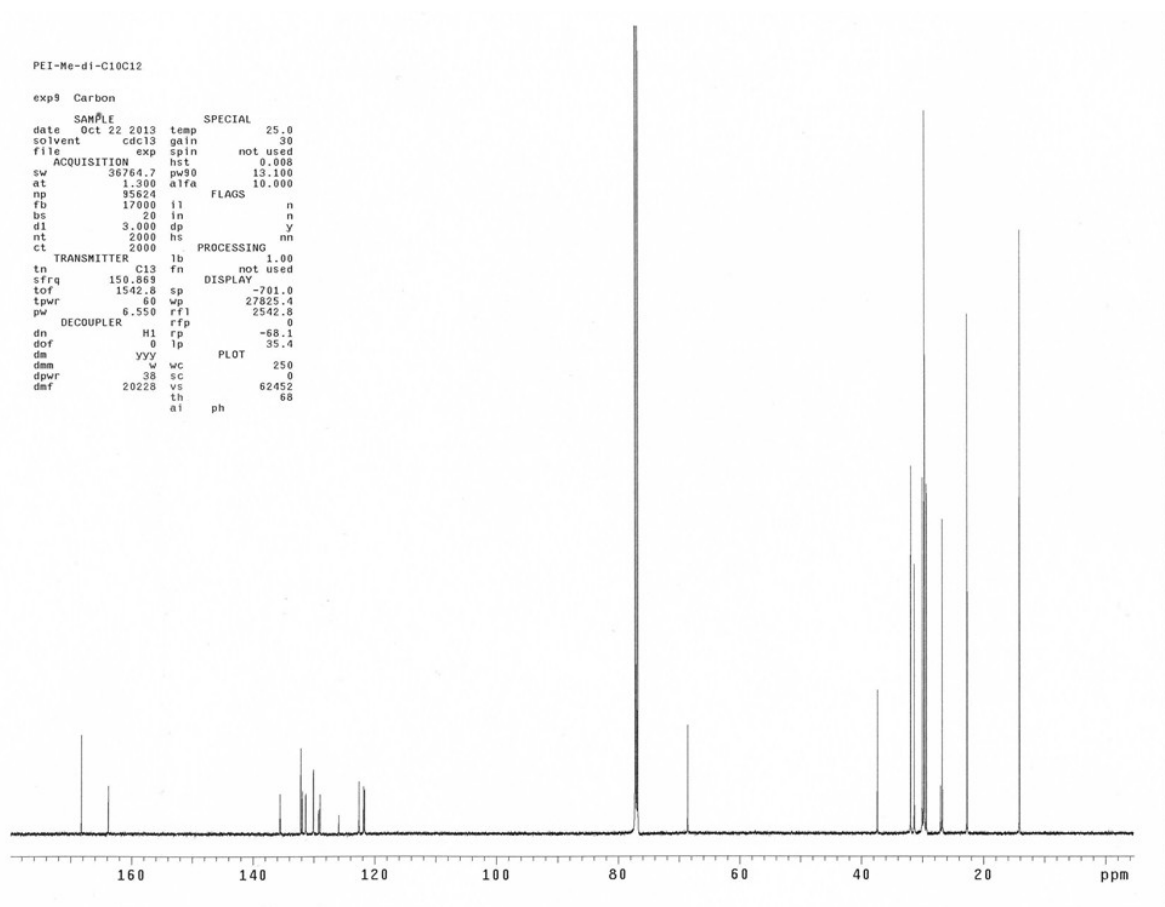


Figure S4. ^{13}C NMR spectrum of **2**

4. Summary of WAXD diffraction positions of PEA 1 and PEI 2

Table S2. WAXD diffraction positions of PEA 1

index	2θ ($^\circ$)	measured d-spacing (nm)	Calculated d-spacing (nm)	deviation (nm)
(100)	2.35	3.76	3.77	-0.01
(110)	4.10	2.16	2.18	-0.02
(200)	4.68	1.89	1.88	0.01
(210)	6.25	1.41	1.42	-0.01
(300)	8.30	1.26	1.26	0
(001)	4.83	1.83	1.803	0.027

(002)	9.85	0.898	0.902	0.004
(004)	19.85	0.4473	0.4509	-0.0036
(005)	24.69	0.3606	0.3606	0
(006)	29.60	0.3018	0.3006	0.012

Table S3. WAXD diffraction positions of PEI 2

index	2 θ (°)	measured d-spacing (nm)	Calculated d-spacing (nm)	deviation (nm)
(100)	2.87	3.08	3.08	0
(110)	4.10	1.77	1.77	0
(200)	4.68	1.53	1.54	-0.01
(210)	6.25	1.16	1.16	0
(300)	8.30	1.03	1.03	0
(001)	25.04	0.3563	0.3563	0

5. Polarized light microscopic pictures of PEA 1

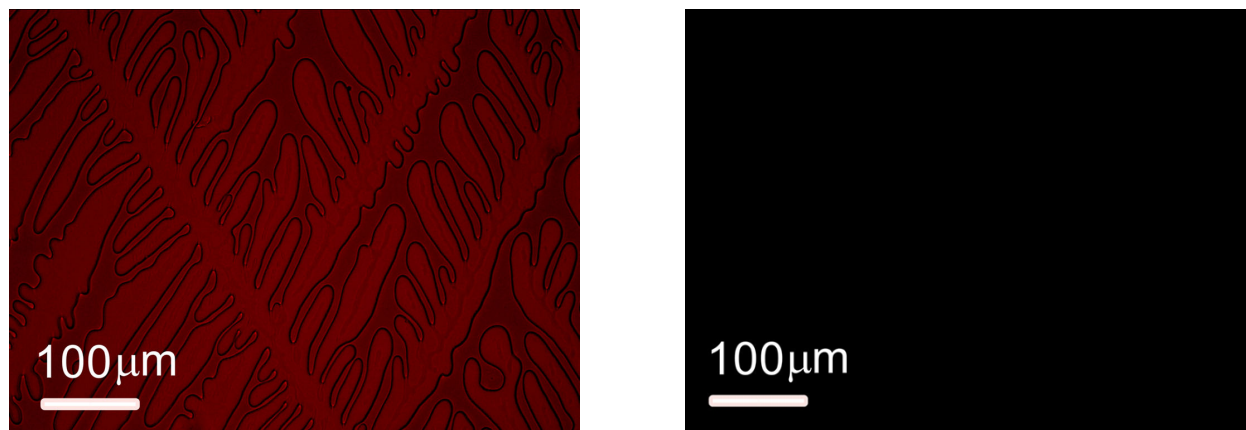


Figure S5. Polarized light microscopic pictures of PEA 1 during slow cooling from the isotropic state. Both pictures were taken on the same area of an ITO glass sandwiched sample film at the same temperature (203.0 °C). The analyzer was slightly uncrossed (67.5 °) with respect to the polarizer in the picture on the left in order to

visually confirm the developing of the BSDCLC phase. The picture on the right shows complete darkness when analyzer is at 90 ° position relative to the polarizer, indicating homeotropic alignment of the sample film. The homeotropic alignment is retained while cooling down to RT as supported by the PLM pictures and 2D XRD pattern (Figure 1f).

6. UV-Visible spectra of PEA 1 and PEI 2

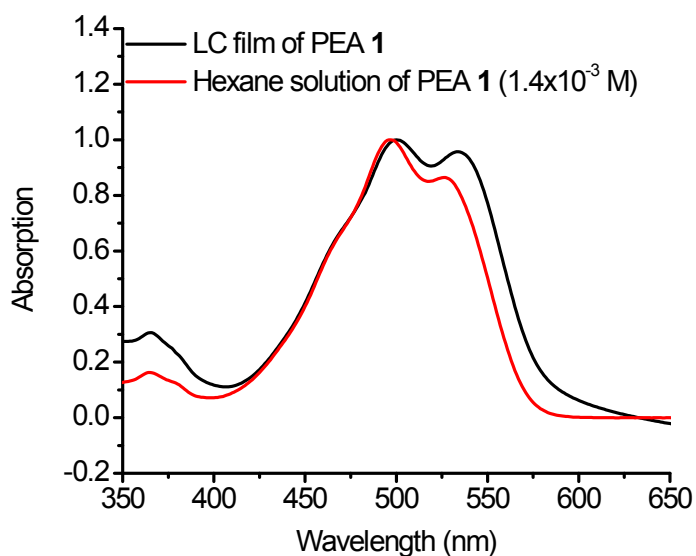


Figure S6. Normalized UV-Visible spectra of LC film and concentrated hexane solution (1.4×10^{-3} M) of PEA **1** at RT. The similarity between two spectra suggests the extensive aggregation of **1** at relatively high concentration.

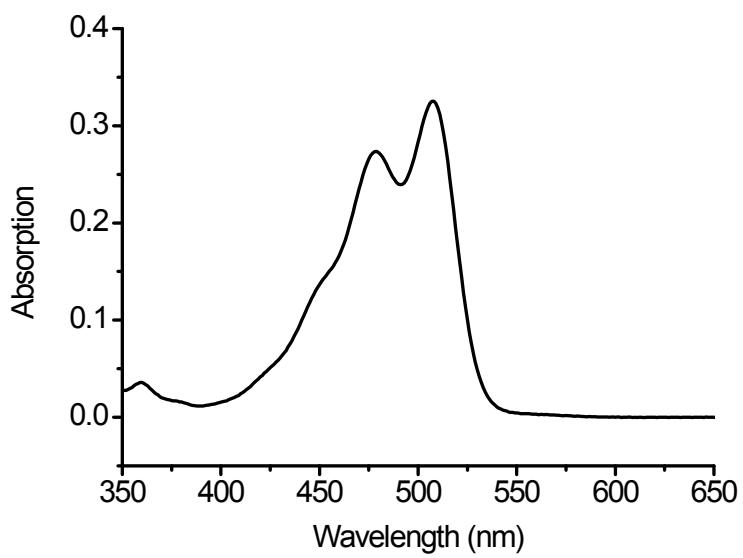


Figure S7. UV-Visible spectrum of PEA **1** in chloroform solution (2.1×10^{-6} M) at RT

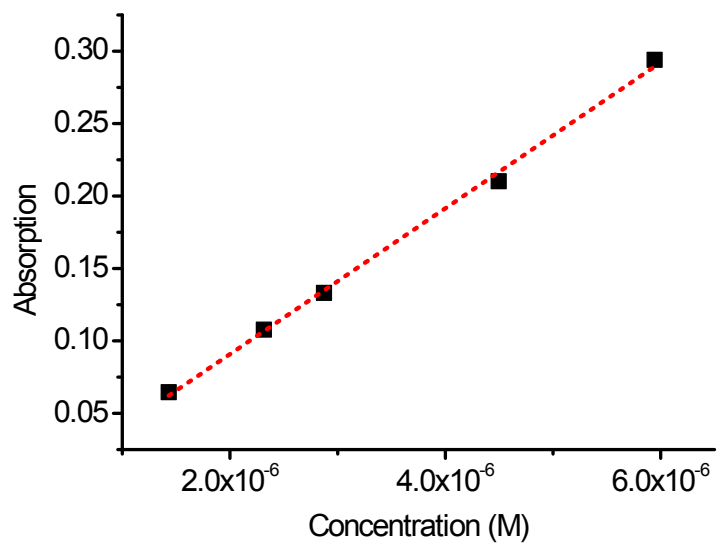


Figure S8. Linear fit of UV-Visible absorptions at 498 nm of hexane solutions of PEA **1** showing the concentration independent nature at low concentration, indicating unassociated **1** molecules

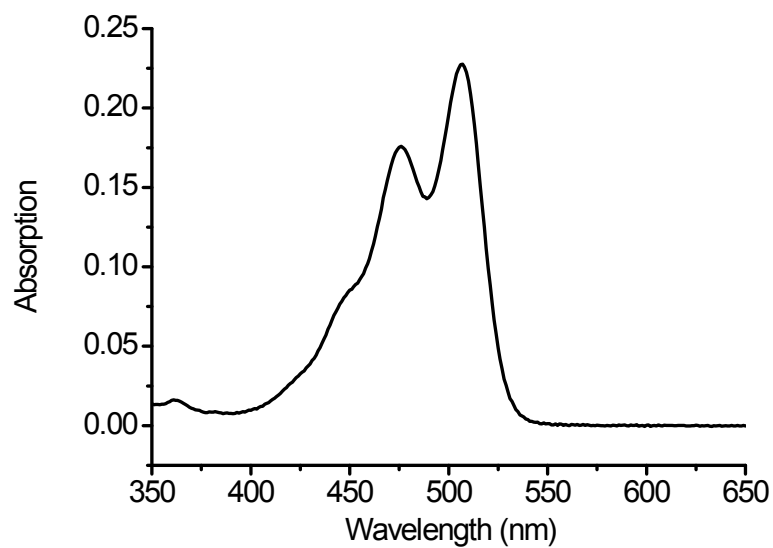


Figure S9. UV-Visible spectrum of PEI **2** in chloroform solution (4.7×10^{-6} M) at RT

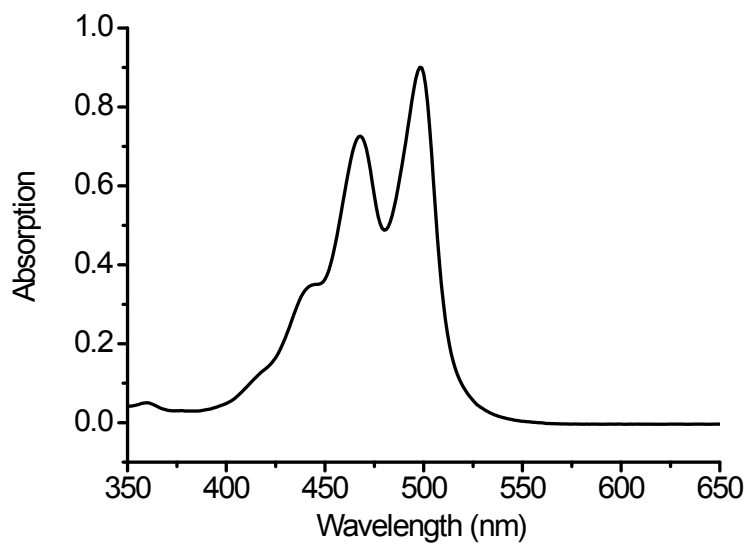


Figure S10. UV-Visible spectrum of PEI **2** in hexane solution (9.5×10^{-5} M) at RT. The spectrum is nearly identical to that of chloroform solution at a much lower concentration, indicating unassociated PEI **2** even at high concentration.

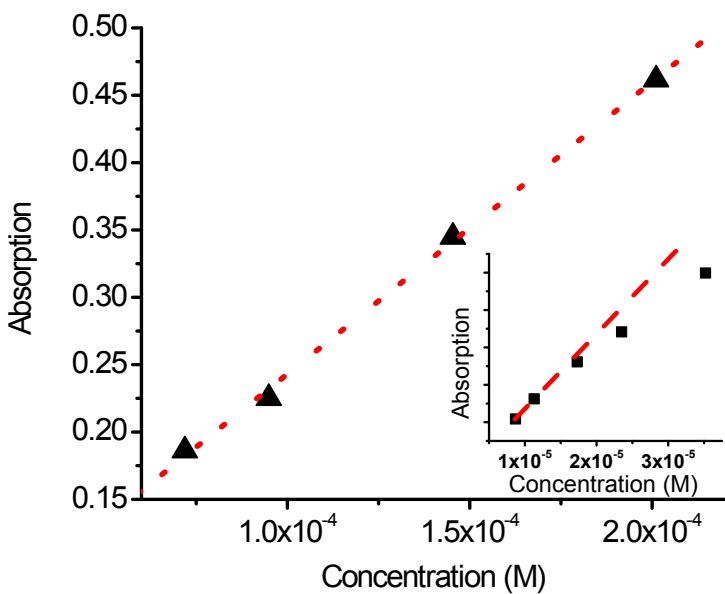


Figure S11. Linear fit of UV-Visible absorptions at 498 nm of hexane solutions of PEI **2** showing the concentration independent nature. The inset shows the concentration dependent nature of PEA **1** molecules in hexane solution in an even lower concentration range, due to strong aggregation. Note that PEI **2** molecules completely dissociate and become single molecularly dissolved at a much higher concentration (see Figure S8) compared to PEA **1**.

7. Fluorescence spectra of PEA **1**

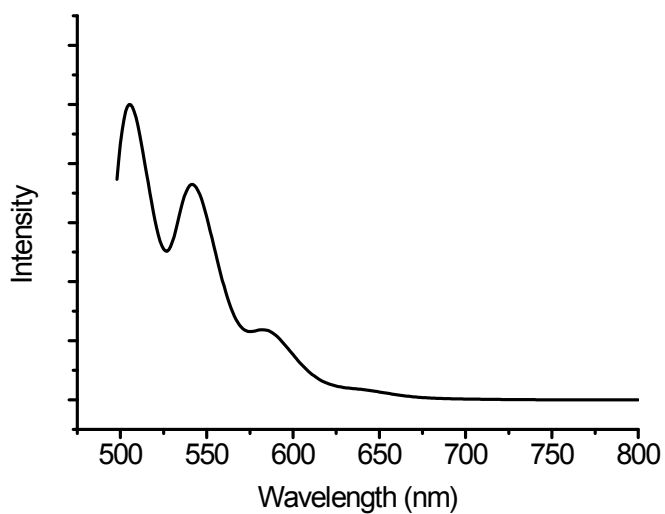


Figure S12. Fluorescence spectrum of unassociated PEA 1 in hexane solution (5.9×10^{-6} M)

8. FT-IR spectra of LC film and hexane solutions of PEA 1

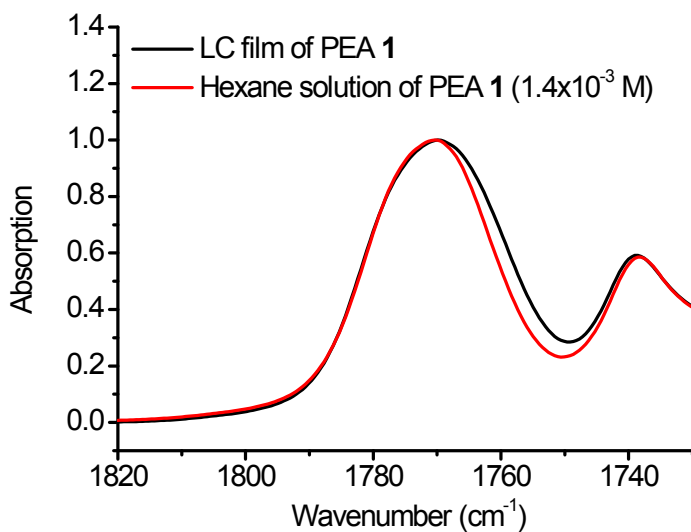


Figure S13. Normalized FTIR spectra of LC film and concentrated hexane solution (1.4×10^{-3} M) of PEA 1 at RT.

The nearly identical spectra indicate strong resemblance of dipole-dipole interactions and chemical environments of anhydride groups in both concentrated hexane solution and DCLC phase of PEA 1, which implies a similar aggregation structure in both cases.

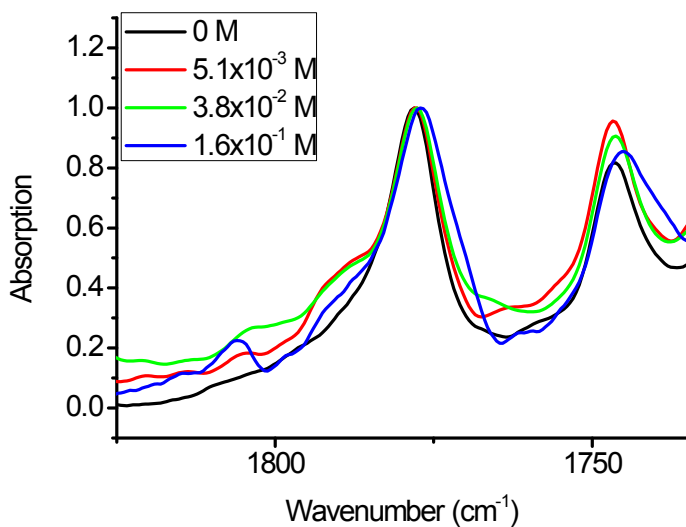


Figure S14. Normalized FTIR spectra of 8×10^{-6} M hexane solutions of PEA **1** at RT with different concentrations of naphthalene (concentrations are shown in the legend). PEA **1** is single molecularly dissolved at 8×10^{-6} M. At the highest naphthalene concentration, there are around 20000 naphthalene molecules for every PEA **1** molecule in the solution. The fact that the spectrum does not undergo noticeable change with naphthalene concentration suggests that anhydride groups interact weakly with aromatic systems. The poor signal to noise ratio is due to the interference from several naphthalene IR absorption bands.

9. DSC traces and 1D and 2D X-ray diffraction patterns of PEI **2**

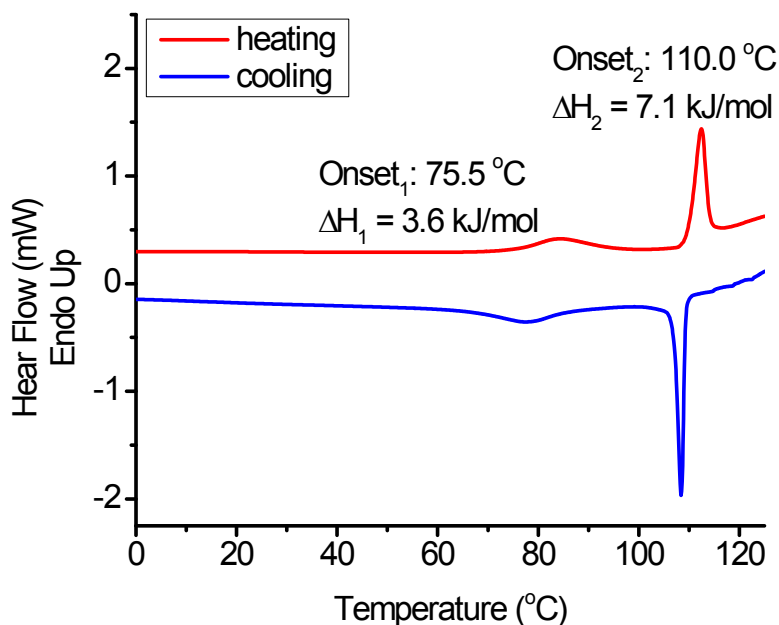


Figure S15. DSC traces (ramp rate = 10 °C/min) and transition parameters of PEI **2**

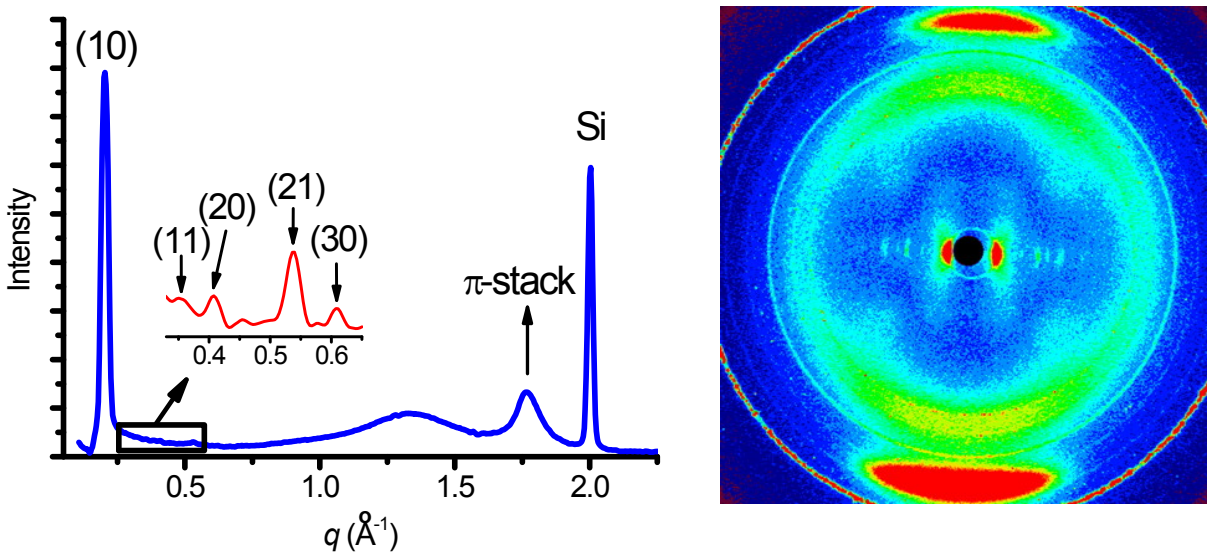
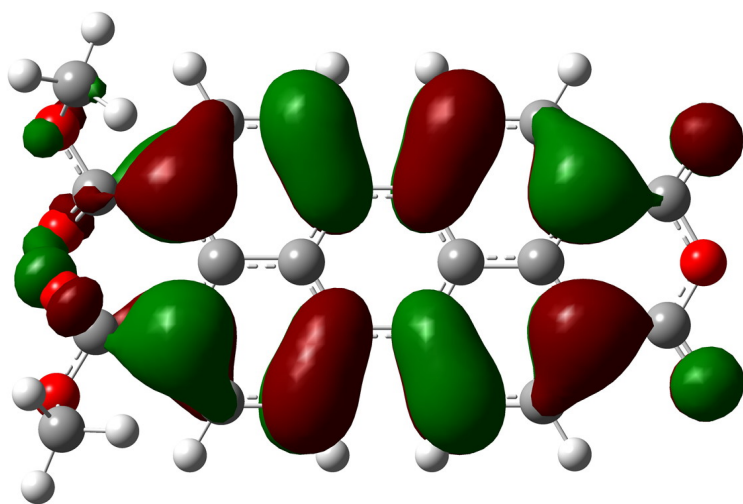
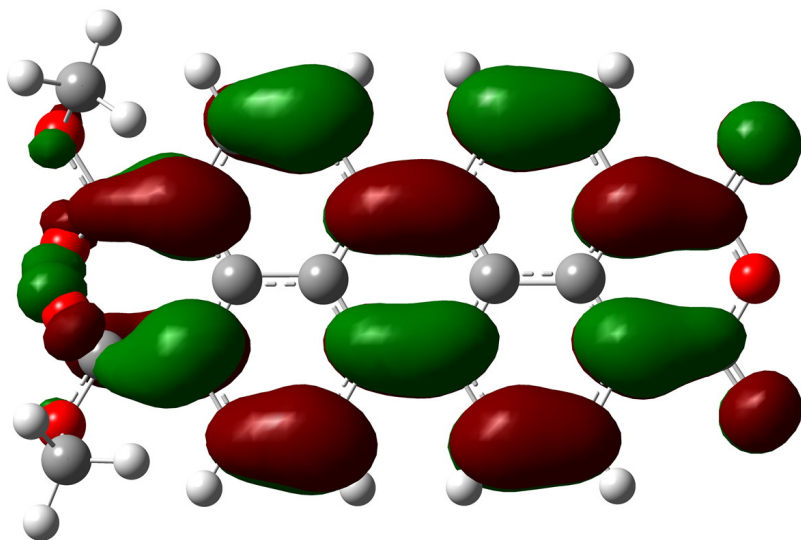


Figure S16. 1D integration (left) and 2D (right) wide-angle X-ray diffraction pattern of PEI **2** (collected at 99 °C). Diffraction rings on the 2D pattern at 1.276, 1.407, 1.573, 1.721, 1.857 \AA^{-1} are due to the aluminum foil which was used as the substrate of PEI **2** film at high temperature. PEI **2** exhibits a multi-stack DCLC phase between 84 and 112 °C. The small-angle diffractions in Figure S16 were indexed as (10), (11), (20), (21) and (30) diffractions of a 2D hexagonal lattice with $a = 3.559$ nm. Assuming the density of PEI **2** to be around 1 g/cm^3 at 99 °C, a two- π -stacks-per-column structure can be inferred.

10. Frontier Molecular Orbitals and Inter-Stack Orbital overlap



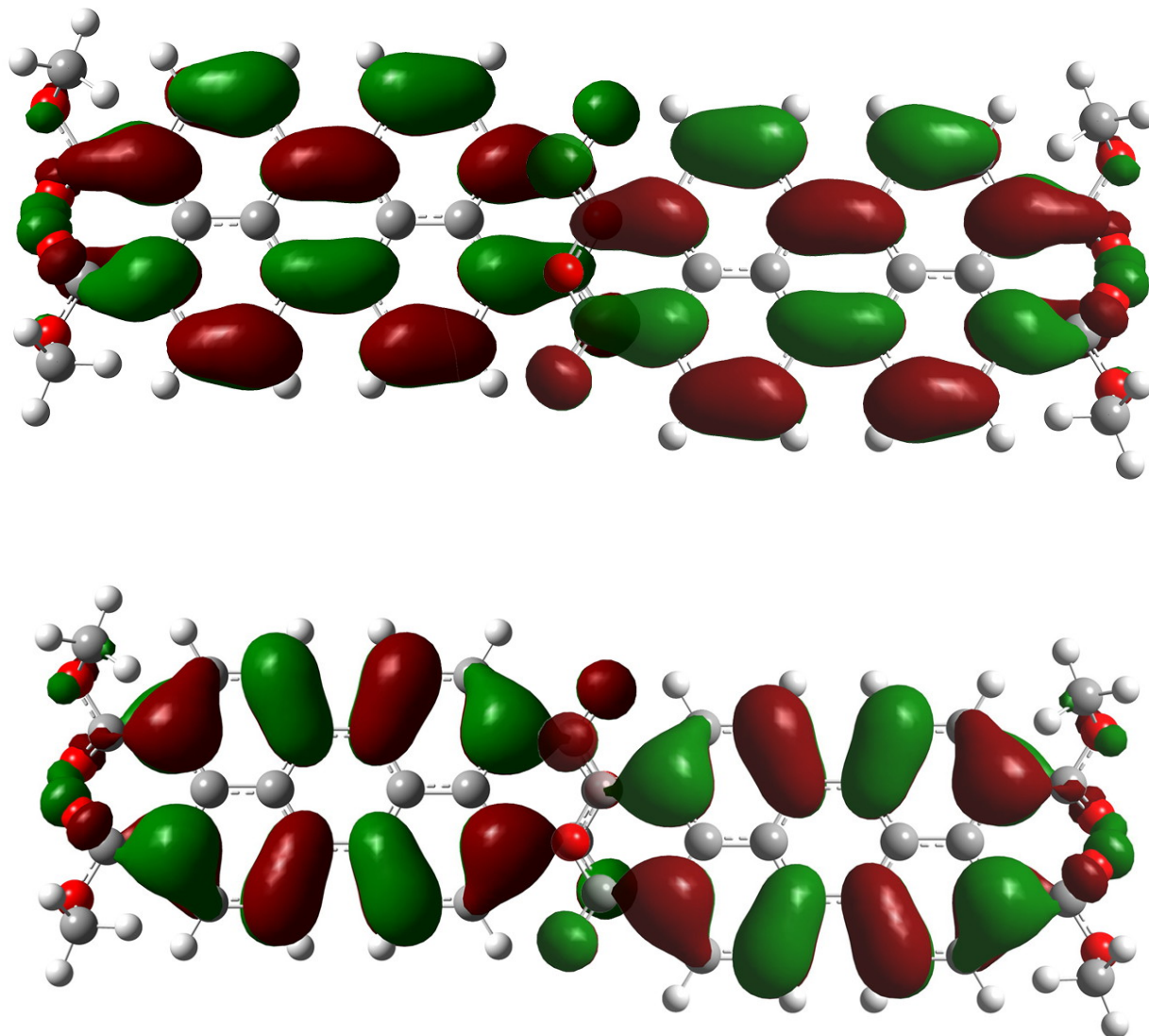


Figure S17. Quantum chemical calculated frontier molecular orbitals (DFT B3LYP) of PEA **1**. From top to bottom: LUMO, HOMO and overlap of LUMO and HOMO as the result of dislocated overlap of two anhydride groups which give rise to ISEC. Note the phase difference on two sides (the view of the opposite phase is sometimes blocked) of the molecular plane and the **in phase** overlap between two anhydride groups.

11. Detailed simulation procedure

Molecular modeling was carried out using a Cerius 2 software package (version 4.10) with COMPASS force field. A model compound (**1M**) was generated. Because the diffraction data indicated that alkyl chains are

disordered, they were replaced by 2-methyl propyl groups, giving the model compound **1M**. When the formation of perylene π -stacks is concerned, a 2-methyl propyl group has essentially the same steric demand as the branched alkyl group in **1**. Therefore both the mesogen-related interactions and flexible chain steric hindrance of **1** involved in intra-column organization can be well represented by **1M**. The energy (1750 kJ/mol) of isolated **1M** molecules in its lowest-energy conformation (Figure S18) was found by adjusting dihedral angles systematically followed by energy minimization. It was used as the reference point to estimate the strength of intermolecular interactions in different structures. Then unit cells were built using Cerius 2 crystal builder. The **a** and **b** parameters of unit cells were set as 6 nm so that inter-column interactions can be neglected, as only intra-column packing is of our interest. As the proposed structure is a composite structure involving both 3 π -stack and 4 π -stack modes, packing of **1M** was first explored in simple 3 π -stack and 4 π -stack modes, respectively.

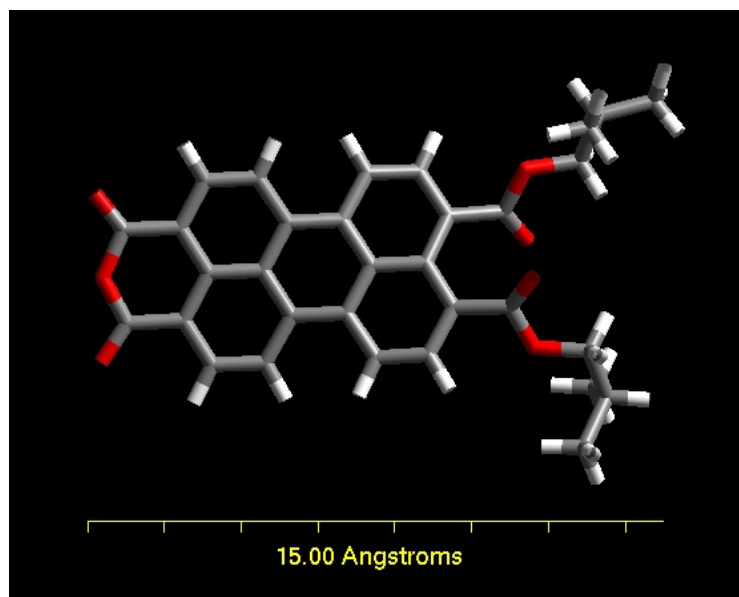


Figure S18. Energy minimized conformation of an isolated **1M** molecule.

For the unit cell with 3 π -stack packing mode, a P3 symmetry was assigned at the beginning. The asymmetric unit includes two **1M** molecules, one on top of the other, with the anhydride side pointing to the center of the column. At the beginning, the perylene π -stack separation was set at 0.3606 nm, as experimentally determined by X-ray diffraction. Thus the cell parameter **c** = 0.7212 nm. However, with the 0.3606 nm stack spacing, the application of energy minimization leads to a structure with the perylene ring plane at a significant

angle with respect to the **ab** plane, which does not agree with the experimental observations. To solve this problem, we set the π -stack spacing first at 0.32 nm (**c** = 0.64 nm). Subsequently, the energy of cell is minimized with high convergence while all cell parameters are fixed during the energy minimization. Upon the completion of the energy minimization at 0.32 nm π -stack spacing, the π -stacking spacing was manually set to 0.3606 nm (**c** = 0.7212 nm). Afterwards, the symmetry of the cell was relaxed to P1 and an energy minimization (100 steps) was performed.

For the unit cell with 4 π -stack packing mode, a P4 symmetry was assigned at the beginning. Then the energy minimization was carried out in the same manner as the 3 π -stack packing mode.

The composite cell was built by combining the 4 π -stack mode (one unit cell) and the 3 π -stack mode (3/2 unit cells). The unit cell parameters were: **a** = **b** = 6 nm, **c** = 1.803 nm, $\alpha = \beta = \gamma = 90^\circ$ with P1 symmetry. Both the 3 π -stack and 4 π -stack parts were placed with perylene rings perpendicular to the **c**-axis and the line connecting two centers coinciding with **c**-axis of the cell. The separation between two parts along the **c**-axis direction is 0.3606 nm. Apparently, the energy of the system depends on the angle by which the three-stack part rotates along the **c**-axis with respect to the four-stack part. To find the angle with the lowest energy, all alkyl groups were removed first since steric repulsion interactions arising from them may overwhelm the interactions of the rigid moieties. Then the energy of the resulted system was calculated as a function of the rotation angle of the 3 π -stack part along the **c**-axis with respect to the 4 π -stack part, with a step size of 1° . Once the lowest energy was found, all atoms involved in the perylene rings and the anhydride groups were set as fixed atoms to avoid their movement during energy minimization of peripheral groups. Subsequently, 2-methyl propyl groups were reattached and an energy minimization was performed with all cell parameters fixed. Finally, upon the convergence of the energy, the motion of all atoms was set as allowed before an energy minimization (100 steps) was performed.

The simulated diffraction pattern was calculated from a single column using the amorphous diffraction module in Cerius 2. The column shown in Figure S19d was built by combining six composite unit cells along the **c**-axis (column axis).

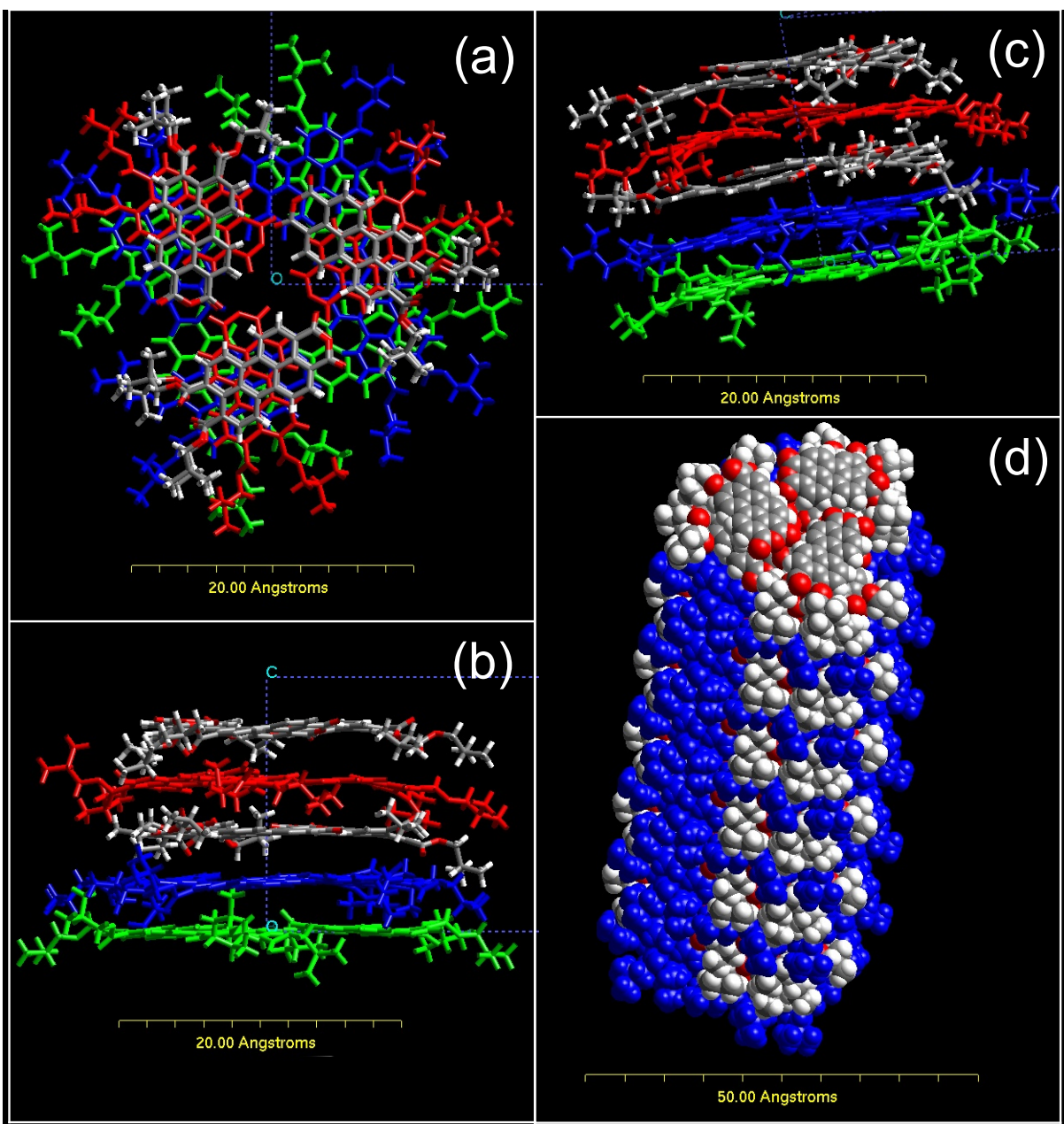


Figure S19. Energy-minimized composite bundled-stack intracolumnar organization of **1M** molecules. (a) top view. (b) side view. (c) tilt view. (d) the single column that was used to calculate the simulated diffraction pattern in Figure 2. In (a), (b) and (c), **1M** molecules were colored stratum-wise. Default color scheme for 1st and 3rd strata, while red, blue and green for 2nd, 4th and 5th strata. In (d), **1M** molecules in the three-stack part were colored according to the default color scheme while those in four-stack part were blue.

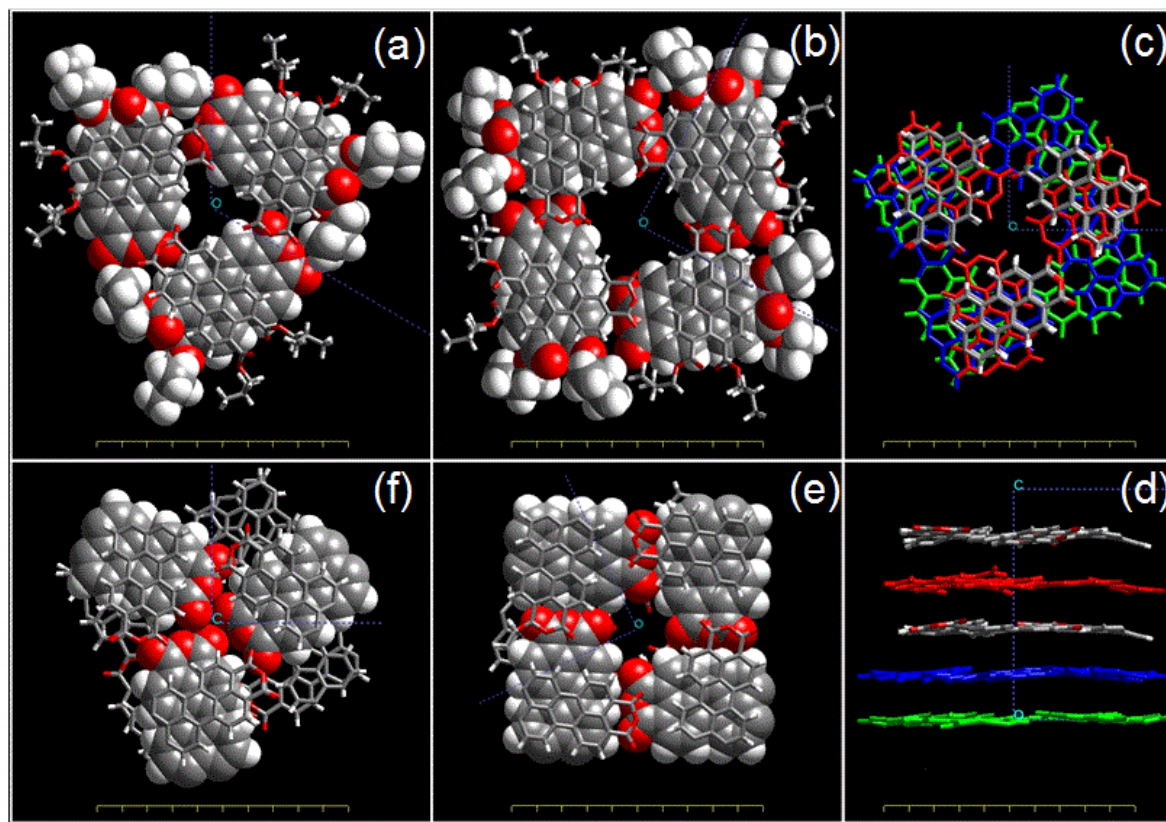


Figure S20. Energy-minimized unit cells viewed along the column axis (except (d) which is a side view). (a) three-stack structure. (b) four-stack structure. (c)-(f) composite structure with the three-stack part (three strata) on the top. Scale bars represent 2 nm. For the composite structure, all peripheral groups were removed for the sake of clarity. Molecules were shown in cylinder models, except in (a), (b), (e) and (f), molecules in the second stratum were shown in space filling models as a means to indicate inter-stack mesogen contact and intra-stack rotation angles. Molecules in (c) and (d) were colored stratum-wise: the default color scheme for 1st and 3rd stratum; red, blue, green for 2nd, 4th and 5th strata, respectively. (e) and (f) show the views from the four-stack and three-stack ends of the composite cell, respectively.

The intra-stack rotation angle is $\sim 99^\circ$ for both three-stack and four-stack structures. Packed **1M** molecules have an average potential energy which is 163 (3 π -stack) or 177 (4 π -stack) kJ/mol lower than an isolated **1M** molecule, due to attractive intermolecular interactions. The calculated average potential energy of **1M** molecules in the composite structure is 159 kJ/mol below that of an isolated **1M**, which indicates that **1M** molecules are experiencing fairly strong attractive intermolecular interactions. However, such interactions are slightly weaker than

those in a simple 3 π -stack or 4 π -stack structure, likely due to the energy cost arising from the 3 π -stack /4 π -stack interfaces. This suggests that the long, flexible alkyl chains should play the key role in driving the formation of the composite structure instead of a simple three-stack or four-stack structure which is more enthalpically favored if long alkyl chains are not considered. We speculate that when packed in the simple three-stack structure, the *n*-alkyl chains of **1** have to adopt a conformation with a relatively large number of gauche dihedrals, which comes with an enthalpy cost leading to a higher free energy. Conversely, when packed in the four-stack structure, the *n*-alkyl chains suffer too few gauche dihedrals, resulting in an entropy penalty. By combining three- and four-stack modes, *n*-alkyl chains are in a conformation with free energy advantage that is more than enough to compensate for the energy cost from the packing discontinuities in the composite structure and makes it the most stable one. This analysis leads to an important implication that peripheral flexible chain engineering may be applied to generate a single-stacking-mode BSDCLC phase.

12. Discussion on the role of flexible long alkyl peripheral chains

Generally speaking, π -stacked discotic mesogens constitute the core of a supramolecular column or the core column. Flexible chains cover the surface of a core column and fill the inter-core column space. In the present case, each **1** molecule can be considered as being equipped with four flexible *n*-alkyl chains. Although it has been suggested experimentally⁵ and shown by molecular dynamics simulations⁵ that interdigitation of flexible *n*-alkyl peripheral chains could occur to a certain extent in a DCLC phase, the occurrence of deep interdigitations, i.e., a part of a core column surface is covered by flexible alkyl chains stemming from an adjacent column, is unlikely, as demonstrated by molecular dynamics simulation studies.⁶ Therefore, the task of covering the core column surface is generally fulfilled by its own *n*-alkyl chains. The ability of an *n*-alkyl chain to cover column core surface is associated with its cross-sectional area, which is conformation-dependent. An *n*-alkyl chain in its all-anti conformation has the smallest cross-sectional area ($\sim 0.188 \text{ nm}^2$ at RT),⁷ therefore it can cover smallest column core surface area. In the event of each *n*-alkyl chain needs to cover a core columnar surface area that is significantly larger than 0.188 nm^2 , gauche dihedrals must be introduced, as the cross-sectional area as well as the ability to cover column core surface area of a *n*-alkyl chain increases with the number of gauche dihedrals. However, the introduction of each gauche dihedral comes with an enthalpy penalty of $\sim 3 \text{ kJ/mol}$, therefore an *n*-alkyl chain with a large number of gauche bonds will be enthalpically disadvantageous. The core column surface areas that each *n*-

alkyl chain is responsible to cover for three structures were estimated, as shown below. The estimated values are 0.276, 0.223 and 0.251 nm² for three-stack, four-stack and the composite structure, respectively. Thus it is expected that those *n*-alkyl chains in the three-stack structure will need the largest number of gauche dihedrals and suffer the greatest enthalpy penalty. At the other end, the *n*-alkyl chains in the four-stack structure need few gauche bonds therefore don't suffer much enthalpy penalty. However, having few gauche bonds leads to a lower entropy. We speculate that in the composite structure, by combining the three-stack and the four-stack modes, each *n*-alkyl chain covers an appropriate amount of core column area and therefore is in the most comfortable conformation. As the result, **1** molecules in the composite structure enjoy the lowest free energy.

The estimation of core column surface areas each *n*-alkyl chain needs to cover near the core surface was done as below.

For three-stack and four-stack structures:

$$A_{pc} = l \times 0.3606 / n$$

n: the effective number of *n*-alkyl chains per stratum in a column (*n* = 12, 16 for three-stack and four-stack structures, respectively); A_{pc} : the column surface area each *n*-alkyl chain needs to cover near the core surface; *l*: the perimeter of the cross-section of a column with **ab** plane. The perimeter was measured along the middle points of carbon-carbon bonds that connect to a methyl group (white line in Figure S21). These points can be approximately considered as the starting points of *n*-alkyl chains in **1**.

$$A_{pc(\text{three-stack})} = 9.18 \times 0.3606 / 12 = 0.276 \text{ nm}^2$$

$$A_{pc(\text{four-stack})} = 9.9 \times 0.3606 / 16 = 0.223 \text{ nm}^2$$

For the composite structure:

$$A_{pc} = [3 \times 3 \times 4 \times A_{pc(\text{three-stack})} + 2 \times 4 \times 4 \times A_{pc(\text{four-stack})}] / (3 \times 3 \times 4 + 2 \times 4 \times 4) = 0.251 \text{ nm}^2$$

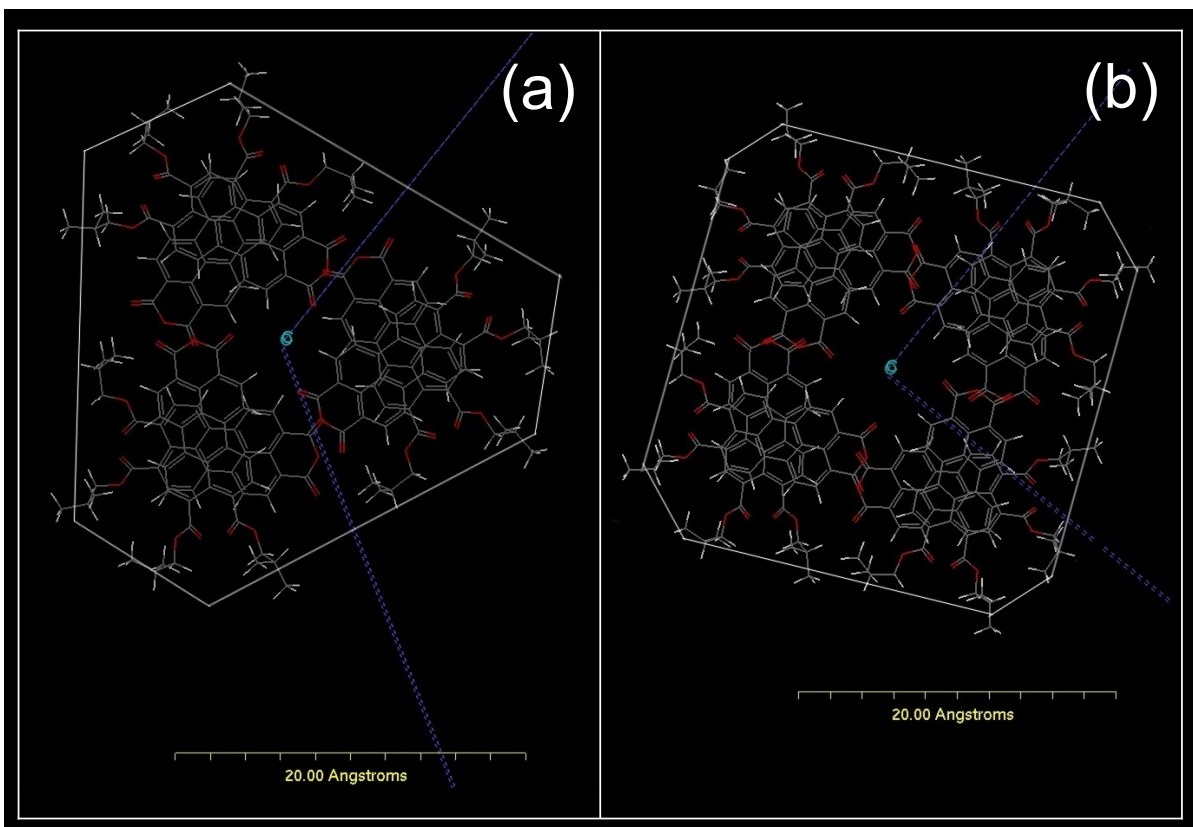


Figure S21. Top views of three-stack (a) and four-stack structures (b). The white polygons mark the paths along which the perimeters were estimated.

13. Conductivity transient of PEA 1 in RT BSDCLC phase by measured by the pulse-radiolysis time resolved microwave conductivity technique

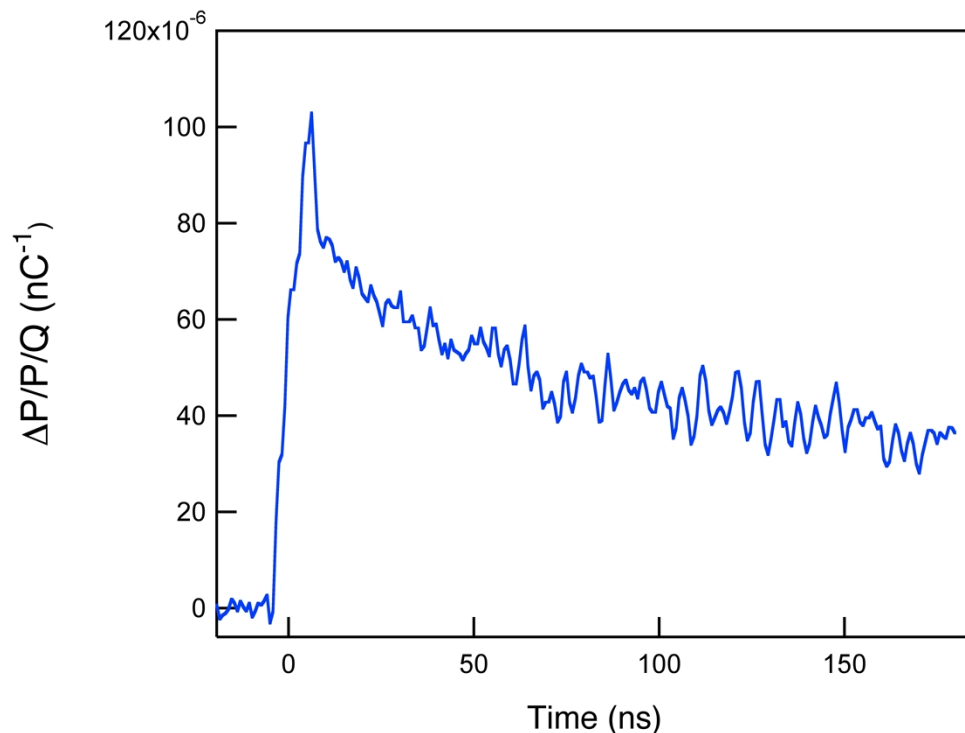


Figure S22. Transient conductivity in PEA **1** in the RT BSDCLC phase upon irradiation with a 5 ns pulse of 3 MeV electrons.

14. References:

1. Warman, J. M.; van de Craats, A. M., Charge Mobility in Discotic Materials Studied by PR-TRMC. *Mol. Cryst. Liq. Cryst.* **2003**, 396, 41-72.
2. Warman, J. M.; de Haas, M. P.; Dicker, G.; Grozema, F. C.; Piris, J.; Debije, M. G., Charge Mobilities in Organic Semiconducting Materials Determined by Pulse-Radiolysis Time-Resolved Microwave Conductivity: π -Bond-Conjugated Polymers versus π - π -Stacked Discotics. *Chem. Mater.* **2004**, 16, 4600-4609.
3. Schouten, P. G.; Warman, J. M.; de Haas M. P.; van Nostrum, C. F.; Gelinck, G. H.; Nolte, R. J. M.; Copyn, M. J.; Zwikker, J. W.; Engel, M. K.; Hanack, M.; Chang, Y. H.; Ford, W. T. The Effect of Structural Modifications on Charge Migration in Mesomorphic Phthalocyanines. *J. Am. Chem. Soc.* **1994**, 116, 6880-6894.

4. Yoshida, Y.; Sakakura, Y.; Aso, N.; Okada, S.; Tanabe, Y., Practical and Efficient Methods for Sulfonylation of Alcohols Using Ts(Ms)Cl/Et₃N and Catalytic Me₃N-HCl as Combined Base: Promising Alternative to Traditional Pyridine. *Tetrahedron* **1999**, *55*, (8), 2183-2192.
5. Allen, M. T.; Diele, S.; Harris, K. D. M.; Hegmann, T.; Kariuki, B. M.; Lose, D.; Preece, J. A.; Tschierske, C. *J. Mater. Chem.* **2001**, *11*, 302-311.
6. (a) Andrienko, D.; Marcon, V.; Kremer, K. *J. Chem. Phys.* **2006**, *125*, 124902. (b) Marcon, V.; Vehoff, T.; Kirkpatrick, J.; Jeong, C.; Yoon, D. Y.; Kremer, K.; Andrienko, D. *J. Chem. Phys.* **2008**, *129*, 094505. (c) Haverkate, L. A.; Zbiri, M.; Johnson, M. R.; Deme, B.; Mulder, F. M.; Kearley, G. J. *J. Phys. Chem. B* **2011**, *115*, 13809-13816.
7. Heinz, H.; Castelijns, H. J.; Suter, U. W., Structure and Phase Transitions of Alkyl Chains on Mica. *J. Am. Chem. Soc.* **2003**, *125*, (31), 9500-9510.